Desalination and Water Treatment
www.deswater.com

doi: 10.5004/dwt.2023.30137

315 (2023) 304–313
December

Preparation and photocatalytic degradation of nickel/carbon microspheres for methylene blue removal

Zhibing Xu, Di Wang, Qixin Wei, Yi Han*, Zhipeng Wang, Nian Liu

School of Resources and Environment, Anqing Normal University, Anqing 246133, China, emails: yihan@whu.edu.cn (Y. Han), 2445115274@qq.com (Z. Xu), 1598243632@qq.com (D. Wang), 576914963@qq.com (Q. Wei), 2505201187@qq.com (Z. Wang), 1977511845@qq.com (N. Liu)

Received 3 August 2023; Accepted 6 November 2023

ABSTRACT

In this paper, carbon microspheres were prepared using glucose and ammonium carbonate at low temperatures, with glucose being the carbon source. In additionally, elemental nickel microspheres were synthesized on the basis of carbon microspheres with nickel as raw material and calcined at high temperature under nitrogen atmosphere. The prepared nickel/carbon (Ni/C) microspheres exhibited optimum morphology and the best photocatalytic performance when the mass ratio of glucose and nickel chloride hexahydrate was 4:1 and the preparation temperature was 500°C, the catalytic decolorization effect of 50 mg of Ni/C microspheres could reach about 76% for 10 mg/L and 50 mL of methylene blue when illuminated for 4 h under daylight. Degradation efficiency increased to 80% at pH = 3. The composites exhibited an energy bandgap of 2.11 eV, which was beneficial for improving the photocatalytic activity. Furthermore, it was found that the active species in the reaction system are mainly •OH radicals.

Keywords: Nickel/carbon microspheres; Photocatalysis; Visible light; Methylene blue

1. Introduction

Water pollution has become one of the major challenges for human society and ecosystems [1–3]. In particular, synthetic organic dyes pose a serious health hazard [4], methylene blue (MB) is widely used in the textile industry for dyeing wool, linen and silk fabrics, and has adverse health and environmental effects [5]. There is an increasing demand for clean and friendly catalytic materials [6–8]. In this regard, nanocomposites are of interest due to their excellent catalytic properties, abundant active centres, high electronic conductivity, low-cost and environmental friendliness [9–14].

In recent years, numerous studies have explored preparation techniques and photocatalytic properties of nickel nanomaterials [15–19]. Jeerapan et al. [20] synthesized nickel nanopowders under a pH of 12.5 based on a hydrated chemical reduction method of nickel ions. Lu et al. [21] used a combination of hydrothermal and ultrasonic methods to synthesize NiS and MoS_2 nanosheets co-modified graphitic C_3N_4 ternary heterostructures and used them for the photocatalytic degradation of antibiotics. Haider et al. [22] used the sol–gel method to synthesize nickel oxide with high photocatalytic activity to treat contamination from potassium permanganate. Among the various preparation methods, hydrothermal synthesis produces nickel nanopowders photocatalysts with small particle sizes and uniform distribution that exhibit excellent catalytic properties under light irradiation [23,24].

Among the various carrier materials, hollow carbon materials can promote ion diffusion and shorten the required diffusion distance of ions [25], one of the carbon materials, such as carbon nanotubes, graphene, and carbon nanorods have high electrical conductivity, all of which are beneficial

* Corresponding author.

to improve the catalytic properties of the composites [26–29]. However, most studies have focused on nickel based on composites and the use of carbon microspheres as carriers has not been fully explored. Therefore, in this paper, hydrothermal synthesis of environmentally friendly carbon microspheres was performed using glucose and ammonium carbonate at low temperatures, whereas nickel/carbon microspheres (Ni/C microspheres) were prepared by high-temperature calcination method. Characterization and qualitative analysis of microspheres using X-ray diffraction (XRD), scanning electron microscopy (SEM), and UV diffuse reflectance tester. In order to analyze the catalytic performance of the catalyst, methylene blue solution was exposed to visible light and the catalytic action was studied. The photocatalytic mechanism of the composites was analyzed by active species capture experiments.

2. Experimental set-up

2.1. Materials

Chemical reagents used in this work were all analytically pure reagents and further purification work was not required. Nickel chloride (content ≥ 98.0%, Tianjin Kaitong Chemical Reagents Co., Ltd., Tianjin, China); p-benzoquinone (content ≥ 98.0%, Shanghai Macklin Biochemical Co., Ltd., Shanghai, China); glucose, ammonium carbonate (content as NH_3 ≥ 40.0%), *tert*-butanol (content ≥ 98.0%), methylene blue (content as dry product ≥ 82.0%) were purchased from Sinopharm Chemical Reagent Co., China. Deionized water was used to prepare all solutions.

2.2. Experimental procedure

A certain mass of glucose and ammonium carbonate was weighed and dissolved in 40 mL of deionized water. The solution of was thoroughly mixed and stirred for 10 min. Then different amounts of nickel chloride (0.5, 1.0, 1.5, and 2 g) were added and the samples were denoted as Ni/C-①, Ni/C-②, Ni/C-③, Ni/C-④. The solution was further stirred for 10 min and poured into a 50 mL polytetrafluoroethylene lined hydrothermal reaction kettle. The brown colored precipitate was filtered, washed with deionized water, and dried at 80°C for 10 h to obtain carbon microspheres. The carbon microspheres were heated to different temperatures (400°C, 500°C, and 600°C) in a tube furnace for 3 h. The samples were then completely calcined and oxidized under nitrogen atmosphere. This was followed by cooling to room temperature to obtain monolithic nickel microspheres, which were denoted as Ni/C-③-400°C, Ni/C-③-500°C, and Ni/C-③-600°C.

2.3. Photocatalytic degradation

In the experiments, 50 mg of catalyst was dispersed into 50 mL (10 mg/L) of MB solution, and the preliminary explorations led to the conclusion that adsorption equilibrium could be reached within 60 min. Therefore, each experiment was carried out for 60 min of the adsorption process before illumination and then, the solution was irradiated with a 300 W xenon lamp. The solution was irradiated with visible light using a metal halide lamp (300 W) during the light reaction process, 3 mL of the solution was taken at 30 min intervals and centrifugal separation operation was carried out and the supernatant was taken to determine the absorbance of the samples at λ = 665 nm on a UV-visible spectrophotometer. The absorbance readings were used to determine the relative concentration of MB, which was given by C/C_0, where, C_0 and C represent the initial concentration of MB and the concentration at time t, respectively. The degradation rates of the catalysts were investigated at different pH (pH = 3, 5, 7, 9, and 11) and different MB concentrations (5, 10, 15, and 20 mg/L). Photocatalytic reactions were performed using a photocatalytic device manufactured by Shanghai Jujing Equipment Co., (Shanghai, China). Fig. 1 shows the preparation steps and photocatalytic schematic of Ni/C.

2.4. Analysis of free radicals

For studying photocatalysis, an experimental procedure similar to that of the photocatalytic degradation outlined in

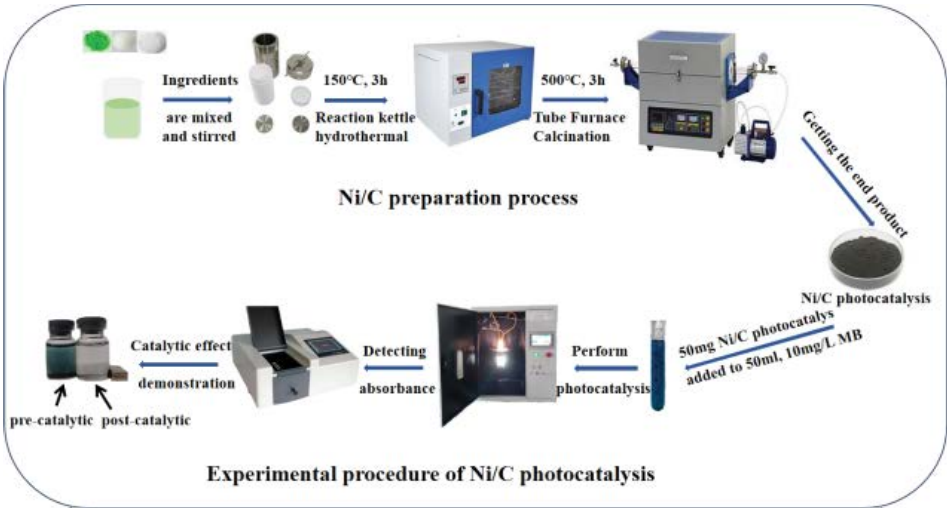

Fig. 1. Ni/C preparation steps and photocatalytic schema.

Section 2.3 – Photocatalytic degradation was used. The catalyst was added to 50 mL of 10 mg/L MB solution and stirred in dark to reach the saturation state of adsorption. In order to determine the contributions of •OH radicals and superoxide radicals $O_2^{-\bullet}$ to the oxidation reaction, *tert*-butanol (TBA) and p-benzoquinone (BQ) were added to the solution for radical trapping experiments [30,31]. In this experiment as well, the absorbance was measured at λ = 665 nm using the UV-Vis spectrophotometer. The relative concentration of MB (C/C_0) was calculated and compared with the relative concentration without the radical trapping agent to determine the contribution of radicals to the oxidation reaction.

2.5. Characterizations of microspheres

The crystal structure of the synthesized samples was characterized using powder XRD (XRD, Bruker D8 Advance, Germany) with CuKα radiation. Further Confirmation of the Composition and Valence of Surface Elements of Prepared Ni/C Materials by X-ray photoelectron spectroscopy (XPS, Thermo Scientific K-Alpha, USA). The particle morphology of the Ni/C microsphere powders was observed using an scanning electron microscope (SEM, ZEISS Sigma 300, Germany). Optical absorption analysis of the samples was carried out on a Shimadzu UV-3600i Plus (Japan) UV diffuse reflectance tester. Qualitative analysis of •OH and $O_2^{-\bullet}$ was performed by electron paramagnetic resonance (EPR, Bruker EMXplus-6/1, Germany), the addition of free radicals during the EPR assay requires the addition of the trapping agent 5,5-dimethyl-1-pyrroline N-oxide (DMPO).

3. Results and discussion

3.1. SEM analysis of Ni/C microspheres

Fig. 2 shows the SEM morphology of the composites synthesized by high temperature calcination and it could be observed that the composites were solid microspheres with nanoparticles attached to the surface. This was realized due to the template of charcoal spheres facilitated by the gradual removal of the polymeric carbon skeleton by oxidation to gas during the calcination process.

The SEM images of the prepared Ni/C microspheres are shown in Fig. 2, and it can be clearly observed that the Ni/C microspheres are spherical in shape. The diameter of Ni/C microspheres is around 3 μm as seen in Fig. 2a. Fig. 2b shows selected regions of the energy-dispersive X-ray spectroscopy (EDS) element mapping, and Fig. 2c and d show the mapping of C and Ni, respectively. As can be seen in the figure, the nickel element was uniformly distributed on the carbon sphere. The elemental spectra and compositions of the Ni/C microspheres found by EDS analysis are given in Fig. 2e, which shows peaks of each element in the nanocomposite, where the presence of nickel can be observed in the carbon microspheres, where the Ni content is about 1.3 atom %.

3.2. XRD analysis of Ni/C microspheres

XRD peaks of the samples obtained after high temperature calcination were consistent with the Ni standard spectrum JCPDS card 04-0850, as shown in Fig. 3. Additionally, Ni diffraction peaks in Fig. 3 are sharper, indicating that the prepared nanometer Ni crystal phase structure was complete with a high degree of crystallinity. The 2θ diffraction peaks of nickel carbide microspheres were in the range of 10° to 80° corresponding to the 44.5°, 51.8°, and 76.3° diffraction peaks of Ni standard card JCPDS card 04-0850. In addition, the XRD spectrum of Ni/C had a broad diffraction peak at 26° which is attributed to the (002) diffraction peak of amorphous carbon [32,33]. Based on the XRD data of Ni/C microspheres, the Ni microcrystal sizes of the three different peak surfaces were determined using the Debye–Schell given by:

$$D = \frac{k\lambda}{B\cos\theta} \tag{1}$$

where K represents Scherrer's constant taken as 0.94. λ, B and θ represent the wavelength of the X-rays (nm), the diffraction peak half-width and the diffraction angle, respectively. The average microcrystal size of the obtained Ni/C microspheres is in the range of 20–27 nm.

3.3. XPS analysis of Ni/C microspheres

In order to further confirm the composition and valence of the elements on the surface of the prepared Ni/C materials, the composites were analyzed by XPS as shown in Fig. 4. It could be seen that the surface of the composite material mainly consists of C, O, and Ni elements, which correspond to the characteristic peaks at the binding energies of 284.0 eV (C1s), 530.0 eV (O1s), and 854.5 eV (Ni2p), respectively, which suggests that Ni was successfully loaded on the carbon microspheres. However, a small amount of divalent Ni was produced because the material was exposed to air [34].

3.4. Optical properties analysis of Ni/C microspheres

The Ni/C microspheres were studied through UV-Visible diffuse reflectance spectroscopy in the wavelength range of 200–2,500 nm, with $BaSO_4$ as the reference, as shown in Fig. 5a. It could be observed that the Ni/C microspheres had strong absorption in the visible light region of 300–700 nm [35], indicating that the electrons on the surface of the microspheres transition to excited state. This improved the quantum efficiency resulting in good visible light photocatalytic reduction performance.

Catalytic efficiency of nanocomposites can be directly or indirectly influenced by optical bandgap. When the bandgap changes, it can produce reactive oxygen species (ROS) or electron–hole relationships (e–h), which play an important role in the photocatalytic process [36]. The optical bandgap can be calculated using the Tauc equation using UV-Vis spectrophotometer data given by:

$$\left(\alpha h\upsilon\right)^2 = A\left(h\upsilon - E_g\right) \tag{2}$$

where α is absorption coefficient, h is Planck constant, and υ is light frequency.

As shown in Fig. 5b, bandgap energy of the synthesized Ni/C microspheres was calculated from the plot of $h\upsilon$ and $(\alpha h\upsilon)^2$ to be 2.11 eV, the bandgap energy of the well-known

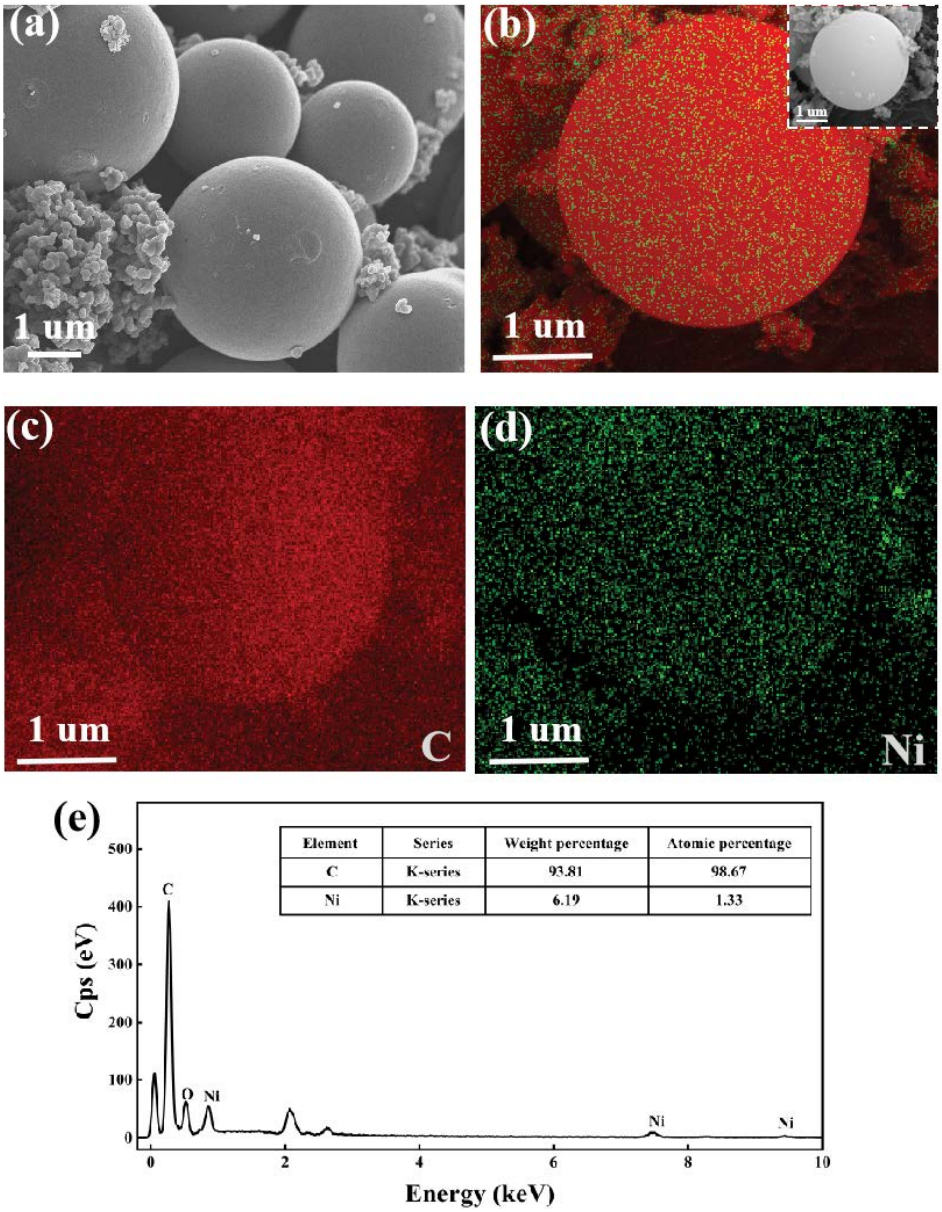

Fig. 2. (a) Scanning electron microscopy images of Ni/C-③ microspheres, (b–d) C, Ni corresponding to the elemental mapping, and (e) elemental spectra and composition of Ni/C-③ obtained by energy-dispersive X-ray spectroscopy analysis.

NiO was 3.7 eV, and the prepared samples were much lower than the bandgap energy of NiO. Typically, the lower the energy bandgap, the more ROS or electron–hole relationship (e–h) will be generated, so the lower the energy bandgap energy is beneficial for improving photocatalytic activity.

3.5. Photocatalytic experiments of Ni/C microspheres

The visible photocatalytic performance of nickel microspheres was analyzed in conjunction with the degradation of MB dye. Figs. 6 and 7 show the influence of nickel microspheres on photocatalytic performance of MB solution under different experimental conditions. It can be seen from Fig. 6 that the catalytic effect of nickel on 10 mg/L MB solution was appreciable when among of nickel was 1.5 and 2.0 g. Since the degradation rate was similar when the amount of nickel was 1.5 and 2.0 g, the optimum nickel concentration was chosen to be 1.5 g. Fig. 7 shows the degradation rate of Ni/C microspheres at different temperatures in 10 mg/L MB solution, where it could be observed that degradation rate of MB at an optimal preparation temperature of 500°C can reach 76%. Photodegradation kinetics of MB has been shown to follow a pseudo primary kinetic law [37–39], so the primary rate constant k for degradation can be plotted against time for $\ln(C_0/C)$ according to Eq. (3):

$$\ln\left(\frac{C_0}{C}\right) = -k \cdot t \tag{3}$$

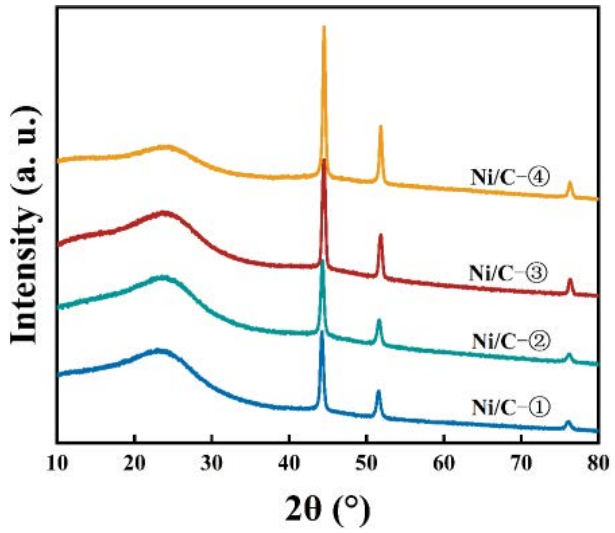

Fig. 3. X-ray diffraction patterns of Ni/C microspheres with different amounts of nickel addition.

Eq. (3) shows the trend of a straight line, which indicated that the degradation process conforms to the first-order kinetic model [40,41]. Figs. 6 and 7 show the kinetic curves of the 10 mg/L MB solution, it could be seen that the nickel concentration of 1.5 g and the temperature of 500°C which demonstrates the best performance. The linear fitting curve yields the following relationship, $y = 0.00545x + 0.000605$, the rate constant (h) of the photocatalytic degradation of MB by Ni/C microspheres was 0.00545. It could be seen from the first-order reaction kinetics that the concentration of reactants decreases exponentially with time. Since $r = kC_0 \exp(-kt)$, the increase of t will not only slow down the reaction rate, but also reduces the consumption of reactants. The photocatalytic degradation of MB was an irreversible reaction, $t \to \infty$, $C \to \infty$, indicating that it taken an infinite time to complete the reaction.

For photocatalysis studies, 50 mg nickel microspheres with the best preparation conditions were added to 50 mL MB solution with concentrations of 5, 10, 15, and 20 mg/L. A 300 W fluorescent lamp was used to illuminate the samples. The degradation rate of the solution during the

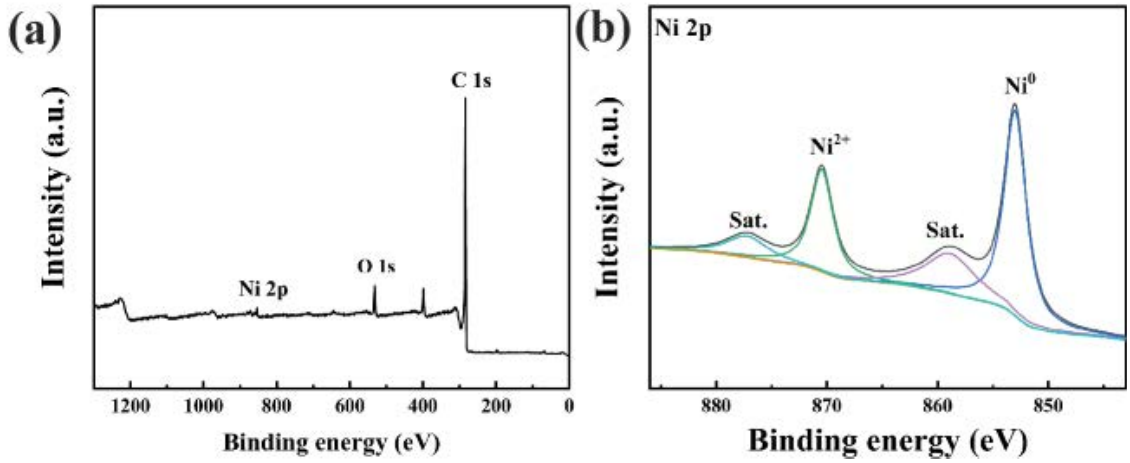

Fig. 4. (a) X-ray photoelectron spectroscopy full spectrum of Ni/C microspheres and (b) X-ray photoelectron spectra of Ni.

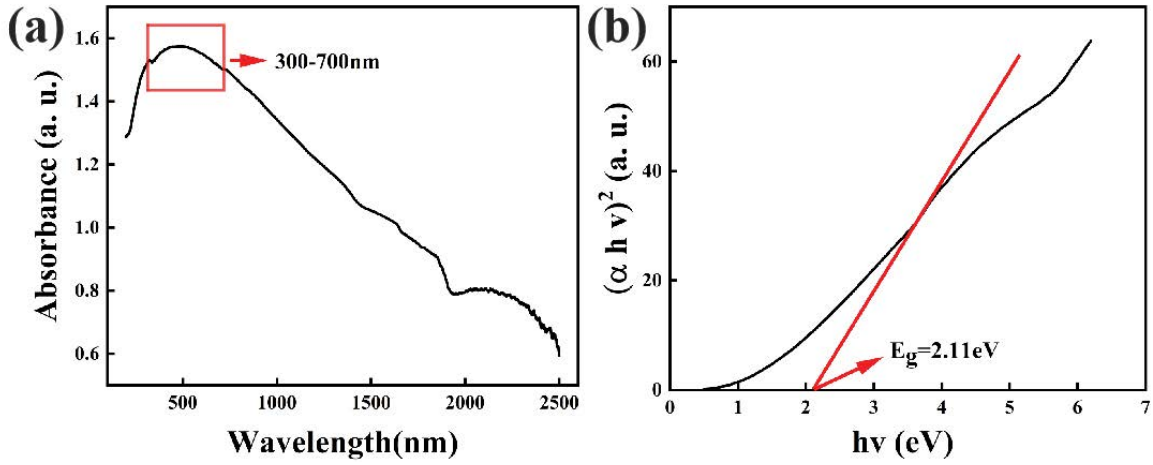

Fig. 5. (a) UV-Visible diffuse reflectance of Ni/C microspheres and (b) bandgap of Ni/C microspheres.

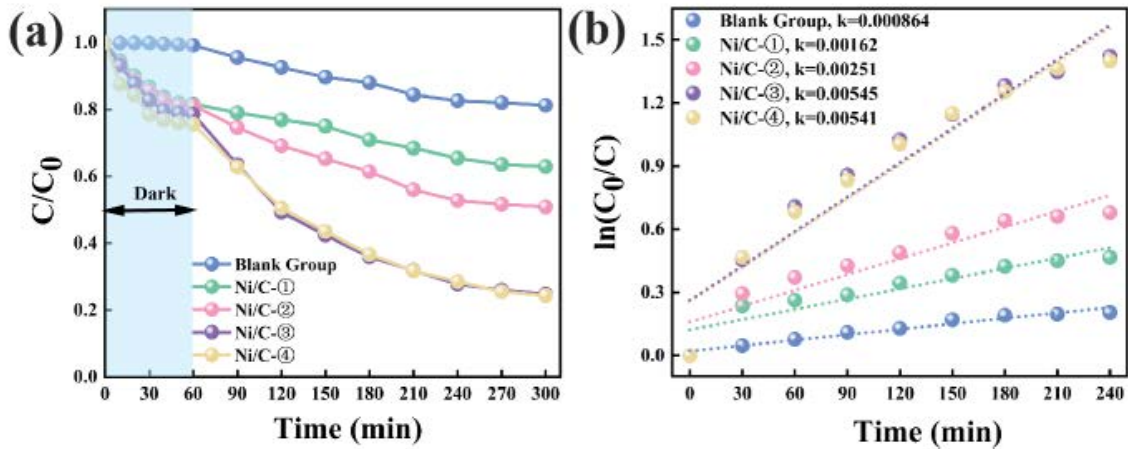

Fig. 6. (a) Degradation rate of methylene blue with different nickel additions and (b) plot of ln(C_0/C) vs. time.

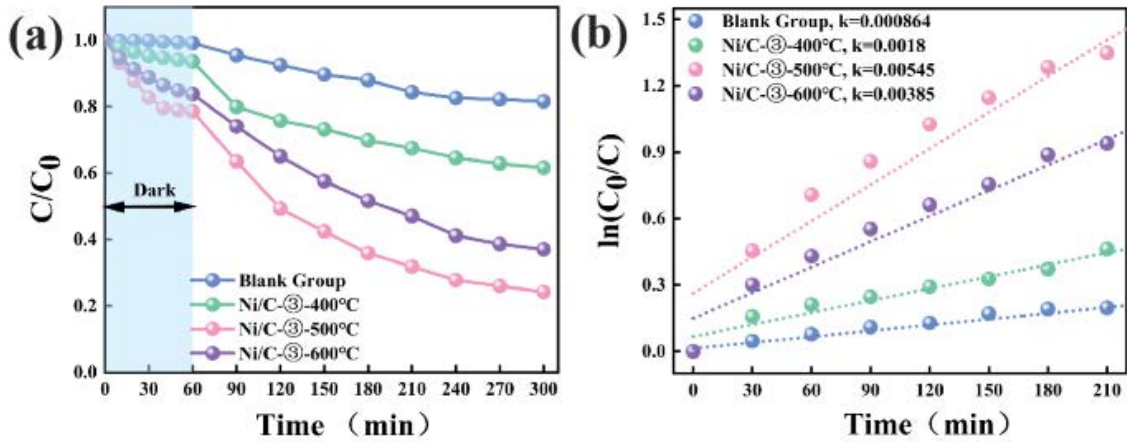

Fig. 7. (a) Degradation rate of methylene blue at different preparation temperatures and (b) plot of ln(C_0/C) vs. time.

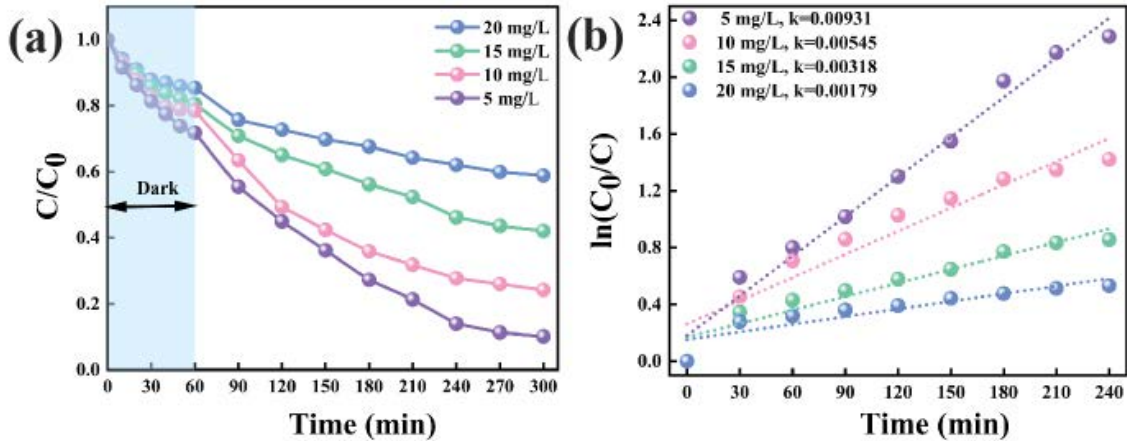

Fig. 8. (a) Degradation rate of different methylene blue concentrations and (b) plot of ln(C_0/C) vs. time.

photocatalytic process as a function of time is shown in Fig. 8. Under an exposure time of 4 h, the degradation rate of 5, 10, and 15 mg/L MB solution reached 90%, 76%, and 58%, respectively. Furthermore, the degradation rate of 20 mg/L methylene blue solution was about 42%. As expected, the reaction rate decreased with increasing concentration,

which is due to the fact that the high concentration of MB is adsorbed on the surface of Ni/C microsphere, resulting in a large number of active sites being blocked, hence the catalytic efficiency decreased. The photocatalytic degradation of MB by different pH (pH = 3, 5, 7, 9, and 11) was also investigated in the same way and the results are shown in Fig. 9. It could be seen that the degradation of MB by different pH under 4 h of fluorescent light catalysis was different, with the best degradation of 80% for the solution at a pH of 3.

3.6. Photocatalytic degradation mechanism

In the photocatalytic degradation of dyes, photons can excite the semiconductor to produce photogenerated electrons and holes. The electrons excited to the bottom of the conduction band generate $O_2^{-\bullet}$ with O_2 being adsorbed on the catalyst surface. This oxidizes the dye that is adsorbed on the catalyst surface, thereby mineralizing it to CO_2 and H_2O. At the same time, the holes remaining at the top of the valence band also undergo oxidation when reacting with the dye [31], or with H_2O and OH^- to generate $^\bullet OH$, which indirectly mineralizes the dye. Trapping agents are generally added to quantify the contribution of $^\bullet OH$ radicals and superoxide radicals $O_2^{-\bullet}$ to the oxidation reaction. Here, TBA and BQ are selected as the trapping agents for $^\bullet OH$ and $O_2^{-\bullet}$ radicals, respectively.

As shown in Fig. 10a, 5 mg/L MB solution with Ni/C-500°C microspheres was stirred in the dark and photocatalyzed under fluorescent light, while 300 mL TBA [42] was added with 100 mL BQ for free radical trapping experiments. The degradation rate of Ni/C-500°C microspheres was observed to significantly decrease from 90% to 55% (17% for MB solution without catalyst) after the addition of TBA. Additionally, the degradation rate of Ni/C-500°C microspheres decreased from 90% to 73% after the addition of BQ, which was not significantly different from the case where the trapping agent was not added. Therefore, it could be concluded that the degradation reaction of MB occurs mainly in solution, and when Ni/C-500°C microspheres were used as photocatalysts. The reactive substances in the reaction system are mainly dominated by $^\bullet OH$ radicals and supplemented by

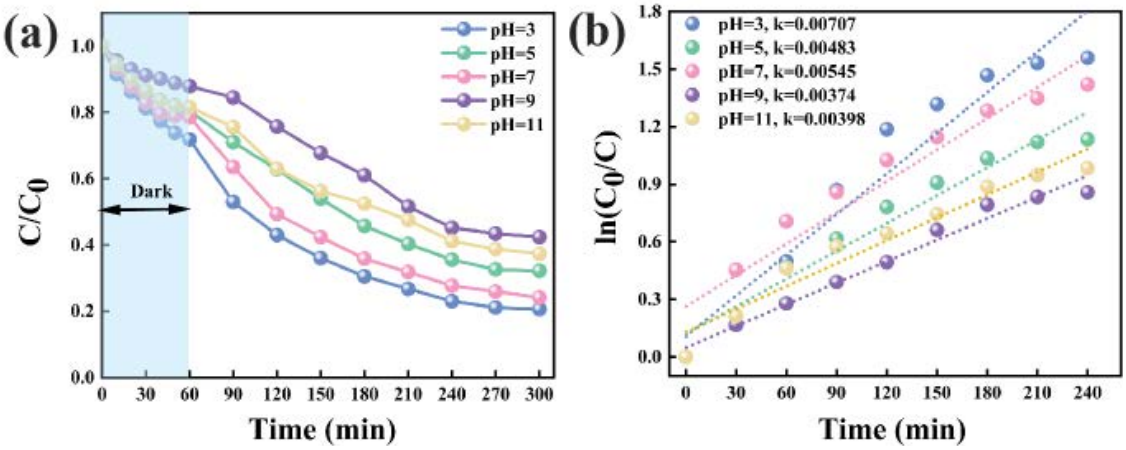

Fig. 9. (a) Degradation rate of different methylene blue concentrations and (b) plot of $\ln(C_0/C)$ vs. time.

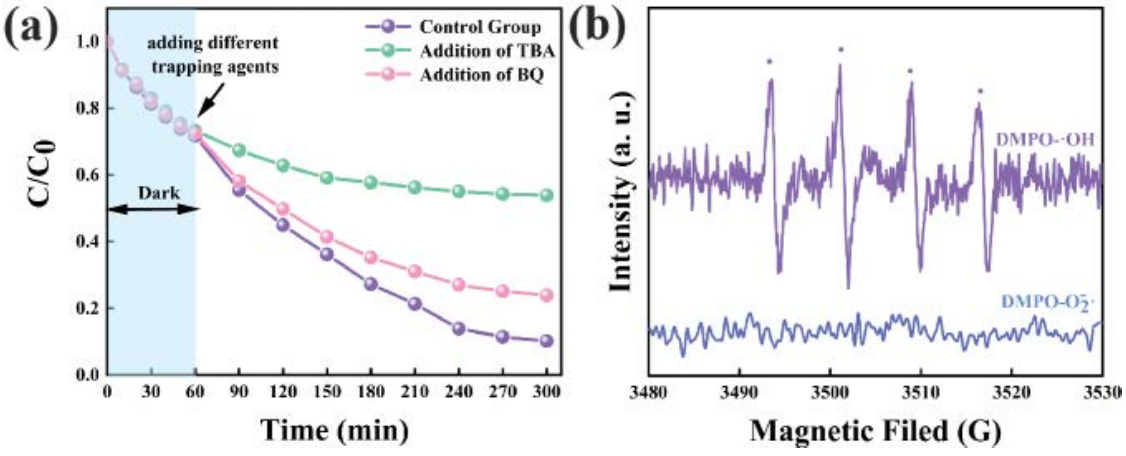

Fig. 10. (a) Effect of adding different trapping agents on the degradation rate of Ni/C microspheres and (b) electron paramagnetic resonance spectra under chloride ion co-existence using 5,5-dimethyl-1-pyrroline N-oxide (DMPO) for $^\bullet OH$.

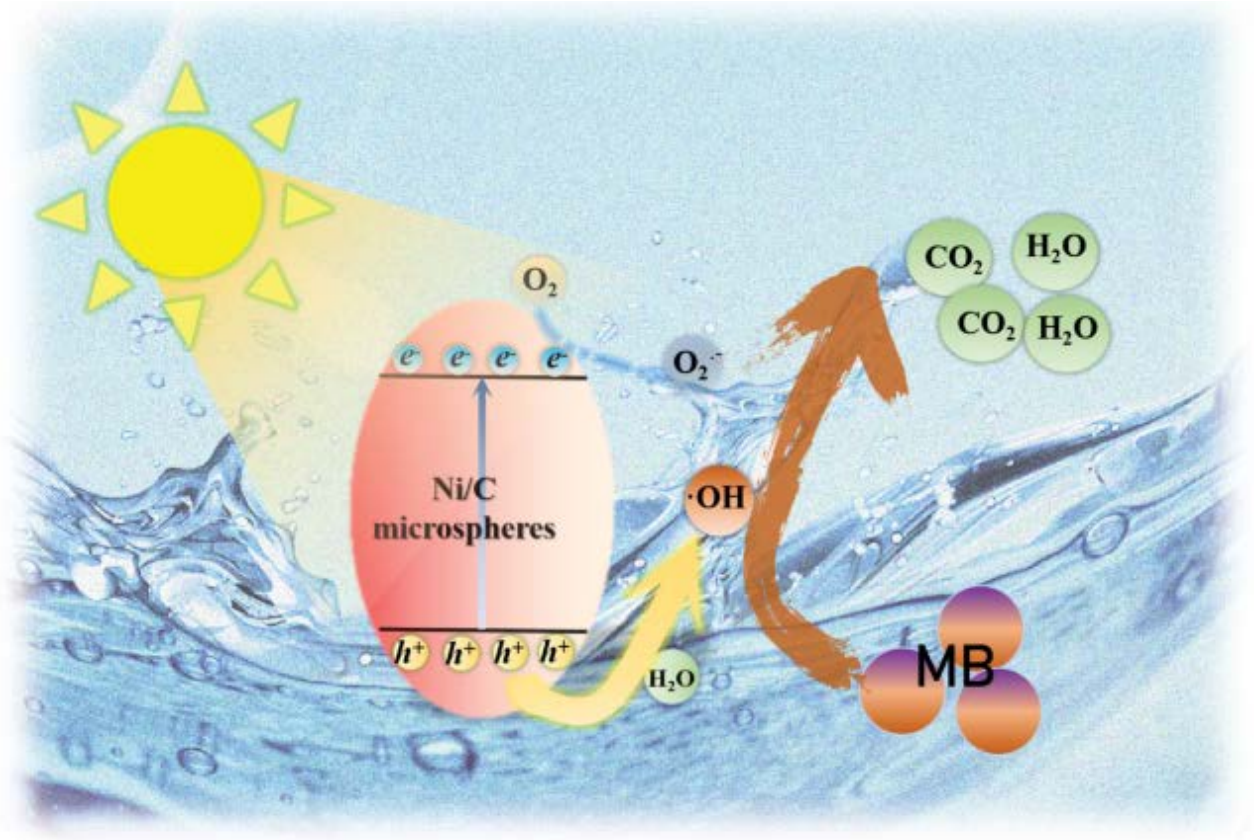

Fig. 11. Schematic diagram of the mechanism of photocatalytic degradation of methylene blue by Ni/C microspheres.

superoxide radicals $O_2^{-\bullet}$. The free radical inhibitor interacted with the generated $^{\bullet}OH$ radicals and $O_2^{-\bullet}$ radicals, thus interrupting the entire free radical chain reaction, which has a great influence on the degradation of MB. Fig. 10b shows the electron paramagnetic resonance (EPR) spectra of the added Ni/C-500°C microspheres under light for 30 min, where the number of $^{\bullet}OH$ radicals was observed to significantly increase after the addition of the prepared catalyst, which further confirms that hydroxyl radicals were predominantly responsible for the enhanced photodegradation [43].

Fig. 11 shows the schematic diagram of the photocatalytic reaction mechanism. Theoretically, Ni/C microspheres were sufficient to oxidize OH^- to generate $^{\bullet}OH$, so most of the holes generate $^{\bullet}OH$ to oxidize MB. Furthermore, a small portion of photogenerated holes directly mineralize MB, converting it to CO_2 and H_2O for degradation. Meanwhile, the capture experiment proved that the active species in the reaction system are $^{\bullet}OH$ radicals, with $O_2^{-\bullet}$ only playing an auxiliary role. Therefore, $^{\bullet}OH$ produced by photogenerated h^+ was mostly the main active agent in the photocatalytic process, and $O_2^{-\bullet}$ plays a secondary role in facilitating the photocatalytic process. Both substances had a strong oxidative capacity and could easily degrade methylene blue dyes.

4. Conclusion

In this paper, Ni/C microspheres were prepared, and their catalytic properties were investigated. For the preparation of carbon microspheres, ammonium carbonate was added to the aqueous solution of glucose and nickel chloride hexahydrate. When the mass ratio of carbonic acid to glucose was 1:6, the reaction system was placed in an autoclave and treated at 150°C for 3 h. Carbon microspheres were successfully synthesized, and glucose polymerization was achieved at a lower temperature.

The Ni/C microspheres were prepared after high temperature calcination at a mass ratio of 4:1 between glucose and nickel chloride hexahydrate. A preparation temperature of 500°C yielded good morphological and photocatalytic properties. The catalytic decolorization effect of 50 mg of Ni/C microspheres could reach about 90% for 5 mg/L and 50 mL of methylene blue when illuminated for 4 h under daylight.

Degradation efficiency increased to 80% at pH = 3. The composites exhibited an energy bandgap of 2.11 eV, which was beneficial for improving the photocatalytic activity. The degradation reaction of methylene blue mainly occurs in solution, and when Ni/C microspheres were used as photocatalysts, the active species in the reaction system were mainly $^{\bullet}OH$ radicals.

Credit authorship contribution statement

Di Wang: Data curation, Writing-Original draft preparation; Zhibing Xu: Conceptualization, Methodology, Software; Qixin Wei: Conceptualization, Methodology, Software; Zhipeng Wang: Software, Validation; Nian Liu: Supervision; Yi Han: Writing-Reviewing and Editing.

Declaration of competing interest

The authors declare that they have no known competing financial interests or personal relationships that could have appeared to influence the work reported in this paper.

Acknowledgements

This work was supported by the grants from National Key Research and Development Program of China (No. 2019YFC0408501), Key Project Supported by the Natural Science Foundation of the Higher Education Institutions of Anhui Province (2022AH051049). We gratefully acknowledge all the supports provided.

References

[1] J.J. Wang, L. Tang, G.M. Zeng, Y.Y. Zhou, Y.C. Deng, C.Z. Fan, Y.N. Liu, Effect of bismuth tungstate with different hierarchical architectures on photocatalytic degradation of norfloxacin under visible light, Trans. Nonferrous Met. Soc. China, 27 (2017) 1794–1803.

[2] W. Zhao, Z. Wei, L. Zhang, X. Wu, X. Wang, Cr doped SnS_2 nanoflowers: preparation, characterization and photocatalytic decolorization, Mater. Sci. Semicond. Process., 88 (2018) 173–180.

[3] F.G.F. Abbasi, Removal of cadmium from aqueous solution by nano composites of bentonite/TiO_2 and bentonite/ZnO using photocatalysis adsorption process, Silicon, 12 (2020) 2721–2731.

[4] L. Ren, Z. Tang, J. Du, L. Chen, T. Qiang, Recyclable polyurethane foam loaded with carboxymethyl chitosan for adsorption of methylene blue, J. Hazard. Mater., 417 (2021) 126130, doi: 10.1016/j.jhazmat.2021.126130.

[5] S.A. Mosavi, A. Ghadi, P. Gharbani, A. Mehrizad, Photocatalytic removal of methylene blue using Ag@CdSe/zeolite nanocomposite under visible light irradiation by response surface methodology, Mater. Chem. Phys., 267 (2021) 124696, doi: 10.1016/j.matchemphys.2021.124696.

[6] D.O. Glushkov, K.K. Paushkina, D.P. Shabardin, Co-combustion of coal processing waste, oil refining waste and municipal solid waste: mechanism, characteristics, emissions, Chemosphere, 240 (2020) 124892, doi: 10.1016/j.chemosphere.2019.124892.

[7] Y.C. Chen, Evaluating greenhouse gas emissions and energy recovery from municipal and industrial solid waste using waste-to-energy technology, J. Cleaner Prod., 192 (2018) 262–269.

[8] F. Salimi, V. Valiei, C. Karami, Removal of EBT dye from aqueous solution by modified $MoNiO_4$ adsorbent, Desal. Water Treat., 190 (2020) 340–352.

[9] S. Farhad, A. Mozaffar, K.A. Reza, The effect of NaOH and KOH on the characterization of mesoporous AlOOH in the solvothermal route, Ceramics-Silikáty, 60 (2016) 273–277.

[10] F. Salimi, K. Zarei, C. Karami, Naked eye detection of Cr^{3+} and Ni^{2+} ions by gold nanoparticles modified with ribavirin, Silicon, 10 (2018) 1755–1761.

[11] A. Saravanan, P. Senthil Kumar, R.V. Hemavathy, S. Jeevanantham, M.J. Jawahar, J.P. Neshaanthini, R. Saravanan, A review on synthesis methods and recent applications of nanomaterial in wastewater treatment: challenges and future perspectives, Chemosphere, 307 (2022) 135713, doi: 10.1016/j.chemosphere.2022.135713.

[12] M. Manikandan, Y. Hu, K. Cai, J. Zhang, W. Zhang, M. Niu, J. Shang, X. Wang, Electrochemical performance of hydrothermally synthesized NiO/Co_3O_4 nanocomposites with different mass ratio, Mater. Lett., 283 (2021) 128849, doi: 10.1016/j.matlet.2020.128849.

[13] Y. Zhang, W.W. Guo, T.X. Zheng, Y.X. Zhang, X. Fan, Engineering hierarchical diatom@CuO@MnO_2 hybrid for high performance supercapacitor, Appl. Surf. Sci., 427 (2018) 1158–1165.

[14] C. Wang, X.M. Zhang, X.F. Qian, Y. Xie, W.Z. Wang, Y.T. Qian, Preparation of nanocrystalline nickel powders through hydrothermal-reduction method, Mater. Res. Bull., 33 (1998) 1747–1751.

[15] H.Q. Zhang, G. Zou, L. Liu, H. Tong, Y. Li, H. Bai, A.P. Wu, Synthesis of silver nanoparticles using large-area arc discharge and its application in electronic packaging, J. Mater. Sci., 52 (2017) 3375–3387.

[16] L. Bai, J. Fan, P. Hu, F. Yuan, J. Li, Q. Tang, RF plasma synthesis of nickel nanopowders via hydrogen reduction of nickel hydroxide/carbonate, J. Alloys Compd., 481 (2009) 563–567.

[17] J.L.H. Chau, Synthesis of Ni and bimetallic FeNi nanopowders by microwave plasma method, Mater. Lett., 61 (2007) 2753–2756.

[18] E.A. Abdel-Aal, S.M. Malekzadeh, M.M. Rashad, A.A. El-Midany, H. El-Shall, Effect of synthesis conditions on preparation of nickel metal nanopowders via hydrothermal reduction technique, Powder Technol., 171 (2007) 63–68.

[19] Y. Yu, H. Ma, X.X. Tian, H.L. Du, S. Xia, S.B. Qu, Synthesis and electromagnetic absorption properties of micro-nano nickel powders prepared with liquid phase reduction method, J. Adv. Dielectr., 6 (2016) 1650025, doi: 10.1142/S2010135X16500259.

[20] T.T. Jeerapan, G. Stephanie, R.T. Casey, D.G. Teresa, Synthesis of nickel and nickel hydroxide nanopowders by simplified chemical reduction, J. Nanotechnol., 2014 (2014) 193162, doi: 10.1155/2014/193162.

[21] X.J. Lu, Y. Wang, X.Y. Zhang, G.Q. Xu, Y.C. Wang, NiS and MoS_2 nanosheet co-modified graphitic C_3N_4 ternary heterostructure for high efficient visible light photodegradation of antibiotic, J. Hazard. Mater., 341 (2018) 10–19.

[22] A.J. Haider, R. Al-Anbari, H.M. Sami, M.J. Haider, Photocatalytic activity of nickel oxide, J. Mater. Res. Technol., 8 (2019) 2802–2808.

[23] P. Dhandapani, A.A. Prakash, M.S. AlSalhi, S. Maruthamuthu, S. Devanesan, A. Rajasekar, Ureolytic bacteria mediated synthesis of hairy ZnO nanostructure as photocatalyst for decolorization of dyes, Mater. Chem. Phys., 243 (2020) 122619, doi: 10.1016/j.matchemphys.2020.122619.

[24] Y. Sapna, R. Nutan, S. Kalawati, Synthesis and characterization of NiO/Cr_2O_3 nanocomposite with effective sunlight driven photocatalytic degradation of organic dyes, Environ. Sci. Pollut. Res., 30 (2023) 71957–71969.

[25] M.J. Kim, C.H. Wang, J. Earnshaw, T. Park, N. Amirilian, A. Ashok, J. Na, M. Han, A.E. Rowan, J.S. Li, J.W. Yi, Y. Yamauchi, Correction Co, Fe and N co-doped 1D assembly of hollow carbon nanoboxes for high-performance supercapacitors, J. Mater. Chem. A, 10 (2022) 24056–24063.

[26] M. Kim, K. Firestein, J. Fernando, X. Xu, H. Lim, D. Golberg, J. Na, J. Kim, H. Nara, J. Tang, Y. Yamauchi, Strategic design of Fe and N co-doped hierarchically porous carbon as superior ORR catalyst: from the perspective of nanoarchitectonics, Chem. Sci., 13 (2022) 10836–10845.

[27] S. Xu, M. Niu, G. Zhao, S. Ming, X. Li, Q. Zhu, L.X. Ding, M. Kim, A.A. Asma, S. Mohammed, Y. Yusuke, Size control and electronic manipulation of Ru catalyst over B, N co-doped carbon network for high-performance hydrogen evolution reaction, Nano Res., 16 (2023) 6212–6219.

[28] Z. Lei, Y. Lei, X. Liang, L. Yang, J. Feng, High stable rate cycling performances of microporous carbon spheres/selenium composite (MPCS/Se) cathode as lithium–selenium battery, J. Power Sources, 473 (2020) 228611, doi: 10.1016/j.jpowsour.2020.228611.

[29] A.R. Jahangiri, M. Sedighi, F. Salimi, Synthesis of zinc-sulfate nano particles and detection of their induction time, nucleation rate and interfacial tension, Iran. J. Chem. Chem. Eng., 6 (2019) 45–52.

[30] W. Zhang, M.S. Zhao, X.H. Wang, S.G. Wang, M.M. Gao, Anodic electrocatalytic behavior of graphite supported TiO_2 towards the generation of hydroxyl radicals, Electrochim. Acta, 434 (2022) 141303, doi: 10.1016/j.electacta.2022.141303.

[31] V. Perumal, R. Uthrakumar, M. Chinnathambi, C. Inmozhi, R. Robert, M.E. Rajasaravanan, A. Raja, K. Kaviyarasu, Electron-hole recombination effect of SnO_2–CuO nanocomposite for improving methylene blue photocatalytic activity in

wastewater treatment under visible light, J. King Saud Univ. - Sci., 35 (2023) 102388, doi: 10.1016/j.jksus.2022.102388.
[32] B. Men, Y.Z. Sun, M.J. Li, C.Q. Hu, M. Zhang, L.N. Wang, Y. Tang, Y.M. Chen, P.Y. Wan, J.Q. Pan, Hierarchical metal-free nitrogen-doped porous graphene/carbon composites as an efficient oxygen reduction reaction catalyst, ACS Appl. Mater. Interfaces, 8 (2016) 1415–1423.
[33] H.-O. Hassani, A.W. Fahd, Preparation, characterization and catalytic activity of nickel molybdate ($NiMoO_4$) nanoparticles, Molecules, 23 (2018) 273, doi: 10.3390/molecules23020273.
[34] H. Hui, W.J. Sun, X.M. Hu, Q. Wang, T. Wu, S. An, C.Y. Ding, C.M. Chen, L.H. Huang, N. Wang, Additive WO_2 promotes Ni-based catalyst for hydrogen production from auto-thermal reforming of acetic acid, Fuel, 339 (2023) 126914, doi: 10.1016/j.fuel.2022.126914.
[35] A.G. Gnedovets, V.A. Zelenskii, A.B. Ankudinov, I.V. Tregubova, M.I. Alymov, Synthesis of nanostructured island alumina coatings on the surface of macropores of hierarchically porous nickel, Dokl. Chem., 487 (2019) 519–523.
[36] D. Zeng, C. Yu, Q Fan, J. Zeng, Z. Li, Theoretical and experimental research of novel fluorine doped hierarchical Sn_3O_4 microspheres with excellent photocatalytic performance for removal of Cr(VI) and organic pollutants, Chem. Eng. J., 391 (2020) 123607, doi: 10.1016/j.cej.2019.123607.
[37] C. Gu, C. Cheng, H. Huang, T. Wong, N. Wang, T.Y. Zhang, Growth and photocatalytic activity of dendrite-like ZnO@Ag heterostructure nanocrystals, Cryst. Growth Des., 9 (2009) 3278–3285.
[38] A. Maulidya, Y. Yulizar, R. Bakri, D.O.B. Apriandanu, R.M. Surya, Synthesis and characterizations of $Ce_2Zr_2O_7$–TiO_2 for increased photocatalytic activity toward degradation of methylene blue, Ceram. Int., 48 (2022) 29523–32952.
[39] F. Adnan, S.P. Thanasupsin, Kinetic studies using a linear regression analysis for a sorption phenomenon of 17a-methyltestosterone by *Salvinia cucullata* in an active plant reactor, Environ. Eng. Res., 21 (2016) 384–392.
[40] K.G. Bhattacharyya, S.S. Gupta, Adsorption of a few heavy metals on natural and modified kaolinite and montmorillonite: a review, Adv. Colloid Interface Sci., 140 (2008) 114–131.
[41] V.M. Nkwe, D.C. Onwudiwe, M.A. Azeez, Solvothermal synthesis of pure and Sn-doped Bi_2S_3 and the evaluation of their photocatalytic activity on the degradation of methylene blue, BMC Chem., 15 (2021) 65, doi: 10.1186/s13065-021-00792-9.
[42] Z.W. Gao, D.D. Zhang, Y.S. Jun, Does tert-butyl alcohol really terminate the oxidative activity of $^{\bullet}OH$ in inorganic redox chemistry?, Environ. Sci. Technol., 55 (2021) 10442–10450.
[43] G.C. Wu, W.J. Kong, Y. Gao, Y. Kong, Z. Dai, H.B. Dan, Y.N. Shang, S.Q. Wang, F.J. Yin, Q.Y. Yue, B.Y. Gao, Removal of chloramphenicol by sulfide-modified nanoscale zero-valent iron activated persulfate: performance, salt resistance, and reaction mechanisms, Chemosphere, 286 (2022) 131876, doi: 10.1016/j.chemosphere.2021.131876.